

Article

Actual Evapotranspiration and Biomass of Maize from a Red–Green–Near-Infrared (RGNIR) Sensor on Board an Unmanned Aerial Vehicle (UAV)

Robson Argolo dos Santos ^{1,*}, Everardo Chartuni Mantovani ¹, Roberto Filgueiras ¹,
Elpidio Inácio Fernandes-Filho ², Adelaide Cristielle Barbosa da Silva ¹ and
Luan Peroni Venancio ¹

¹ Department of Agricultural Engineering, Federal University of Viçosa (UFV), Avenue Peter Henry Rolfs, Viçosa 36570-900 MG, Brazil; everardo@ufv.br (E.C.M.); roberto.f.filgueiras@ufv.br (R.F.); adelaide.silva@ufv.br (A.C.B.d.S.); luan.venancio@ufv.br (L.P.V.)

² Department of Soil and Plant Nutrition, Federal University of Viçosa (UFV), Avenue Peter Henry Rolfs, Viçosa 36570-900 MG, Brazil; elpidio@ufv.br

* Correspondence: robson.argolo@ufv.br; Tel.: +55-31-3899-2729

Received: 1 July 2020; Accepted: 14 August 2020; Published: 22 August 2020



Abstract: Surface reflectance data acquisition by unmanned aerial vehicles (UAVs) are an important tool for assisting precision agriculture, mainly in medium and small agricultural properties. Vegetation indices, calculated from these data, allow one to estimate the water consumption of crops and predict dry biomass and crop yield, thereby enabling a priori decision-making. Thus, the present study aimed to estimate, using the vegetation indices, the evapotranspiration (ET) and aboveground dry biomass (AGB) of the maize crop using a red–green–near-infrared (RGNIR) sensor onboard a UAV. For this process, 15 sets of images were captured over 61 days of maize crop monitoring. The images of each set were mosaiced and subsequently subjected to geometric correction and conversion from a digital number to reflectance to compute the vegetation indices and basal crop coefficients (K_{cb}). To evaluate the models statistically, 54 plants were collected in the field and evaluated for their AGB values, which were compared through statistical metrics to the data estimated by the models. The K_{cb} values derived from the Soil-Adjusted Vegetation Index (SAVI) were higher than the K_{cb} values derived from the Normalized Difference Vegetation Index (NDVI), possibly due to the linearity of this model. A good agreement ($R^2 = 0.74$) was observed between the actual transpiration of the crop estimated by the K_{cb} derived from SAVI and the observed AGB, while the transpiration derived from the NDVI had an R^2 of 0.69. The AGB estimated using the evaporative fraction with the SAVI model showed, in relation to the observed AGB, an RMSE of 0.092 kg m⁻² and an R^2 of 0.76, whereas when using the evaporative fraction obtained through the NDVI, the RMSE was 0.104 kg m⁻², and the R^2 was 0.74. An RGNIR sensor onboard a UAV proved to be satisfactory to estimate the water demand and AGB of the maize crop by using empirical models of the K_{cb} derived from the vegetation indices, which are an important source of spatialized and low-cost information for decision-making related to water management in agriculture.

Keywords: aerial remote sensing; vegetation index; K_{cb} ; water balance

1. Introduction

Modern agriculture faces the major challenge of feeding the world's population, which is growing at an accelerated pace and must become fully sustainable in environmental terms [1]. By 2050, twice the current production of food is expected to be needed to fulfill the needs of the population [2]. For this, the use of water resources in agriculture should be intensified in the coming years to facilitate greater

production gains per unit area. According to [3], only 20% of all agricultural areas in the world are irrigated, but these areas are responsible for 40% of the total food production. Additionally, UNESCO (2009) [3] estimated that between 1998 and 2030, there will be a 13% increase in water use in agriculture, resulting in an increase in food production of 36%. Thus, the use of water in agricultural systems is increasing, which makes new technology and innovations necessary for the proper allocation of water resources.

Maize is among the most widely consumed sources of carbohydrates in the world and belongs to the group of plants whose production needs to be increased to supply the estimated population. However, to increase agricultural production with a minimal environmental impact (primarily on water resources), technological innovations will be needed in several areas of agriculture, combined with the expansion of precision farming in medium and small agricultural properties.

Precision agriculture, according to Mulla (2013) [4], involves management a specific site at the correct intensity and at the right time. For this, it is necessary to use techniques that can constantly monitor crops but are operationally effective and economically viable. Remote sensing techniques meet these requirements for precision agriculture [5]. Remote sensing involves using sensors, which collect terrestrial surface information through electromagnetic radiation, at orbital, suborbital, or terrestrial levels [6].

Currently, the use of unmanned aerial vehicles (UAVs) is being studied as an alternative option for suborbital remote sensing, mainly due to their low cost, the versatility in their use and transport, their high spatial resolution, and the absence of the influence of clouds [7]. This fact makes the UAV-sensor set an important technology for precision agriculture in large and—especially—in medium and small agricultural areas.

Among the main types of sensor onboard UAVs, RGNIR (red–green–near-infrared (RGNIR) has the lowest acquisition cost [8], which makes it attractive for use in agriculture. Nevertheless, this sensor has limitations in its number of bands and the probability of noise between them [9,10], as this type of sensor captures wavelengths using only one optical lens. RGNIR is a modified red–green–blue (RGB) sensor; this modification consists of the removal of the near-infrared wavelength blocker and the addition of a filter for this wavelength [9,11]; the related band of the blue wavelength is also often removed. In this way, by using the RGNIR sensor, it is possible to apply vegetation indices based on red and infrared wavelengths. These indices allow one to evaluate, model, and quantify various parameters related to crop growth and development, as well as estimate water conditions at a high spatial resolution, high temporal frequency, and without the influence of cloudiness.

By applying vegetation indices (VIs), the water conditions of a crop can be estimated using the basal crop coefficient (K_{cb}). Past studies demonstrated a reliable relationship between VI and K_{cb} [12–15]. This relationship for exposed soil, according to Campos et al. (2018) [15], usually has a K_{cb} value close to zero, which reaches its maximum when the crop reaches its peak of vegetative vigor, i.e., the VI will reach its maximum. However, these studies were conducted using images of orbital sensors. Thus, it is necessary to evaluate the methodology of K_{cb} from VIs using a suborbital approach, involving an RGNIR sensor onboard a UAV.

Using the estimated values of K_{cb} and the reference evapotranspiration (ET_0), it is possible to determine the potential water demand of a crop in the field [16]. Thus, by adequately quantifying the evapotranspiration rates in the agricultural system, it is possible to replenish the water required by the crop. That is, the replenishment of water should meet the crop's needs, ensuring there is neither a dearth nor excess of water. Moreover, by knowing the evapotranspiration processes associated with vegetation indices and climatic data, it is possible to determine the daily increase in the aboveground dry biomass (AGB) of a crop, since transpiration is related to the entry of CO_2 into the plant, which is converted by the photosynthetic process into biomass [17].

AGB has been estimated via parameters derived from the evapotranspiration processes using data from orbital sensors for maize [18–20], wheat [21], and sorghum [22]. However, there are no studies using the K_{cb} parameters to estimate the maize AGB with an RGNIR sensor onboard a UAV. Therefore,

this study is important because AGB prediction using a low-cost sensor could be applied by small- and medium-sized farmers.

Since water is an important input for agriculture and remote sensing is an important tool in AGB prediction, the present study aimed to apply and evaluate, using an RGNIR sensor onboard a UAV, empirical models based on K_{cb} to estimate the actual crop evapotranspiration via a normalization of the vegetation indices' Normalized Difference Vegetation Index (NDVI) and Soil-Adjusted Vegetation Index (SAVI) values and to apply, using the evapotranspiration parameters, models to estimate the aboveground dry biomass (AGB) of the maize crop.

2. Material and Methods

2.1. Study Area

This study was carried out in an area of 2600 m² located in the “Prof. Diogo Alves de Mello” experimental field, which belongs to the Federal University of Viçosa (UFV) in the municipality of Viçosa, Minas Gerais State, Brazil (Figure 1). According to Köppen’s climatic classification [23], the climate of the region is Cwa (humid subtropical). The maximum average temperature is 26.7 °C, and the minimum average temperature is 15.4 °C, with an average annual accumulated precipitation of 1250 mm [24]. The soil of this area is classified as deep clay-textured *Latosolo Amarelo* (Oxisol) [25].

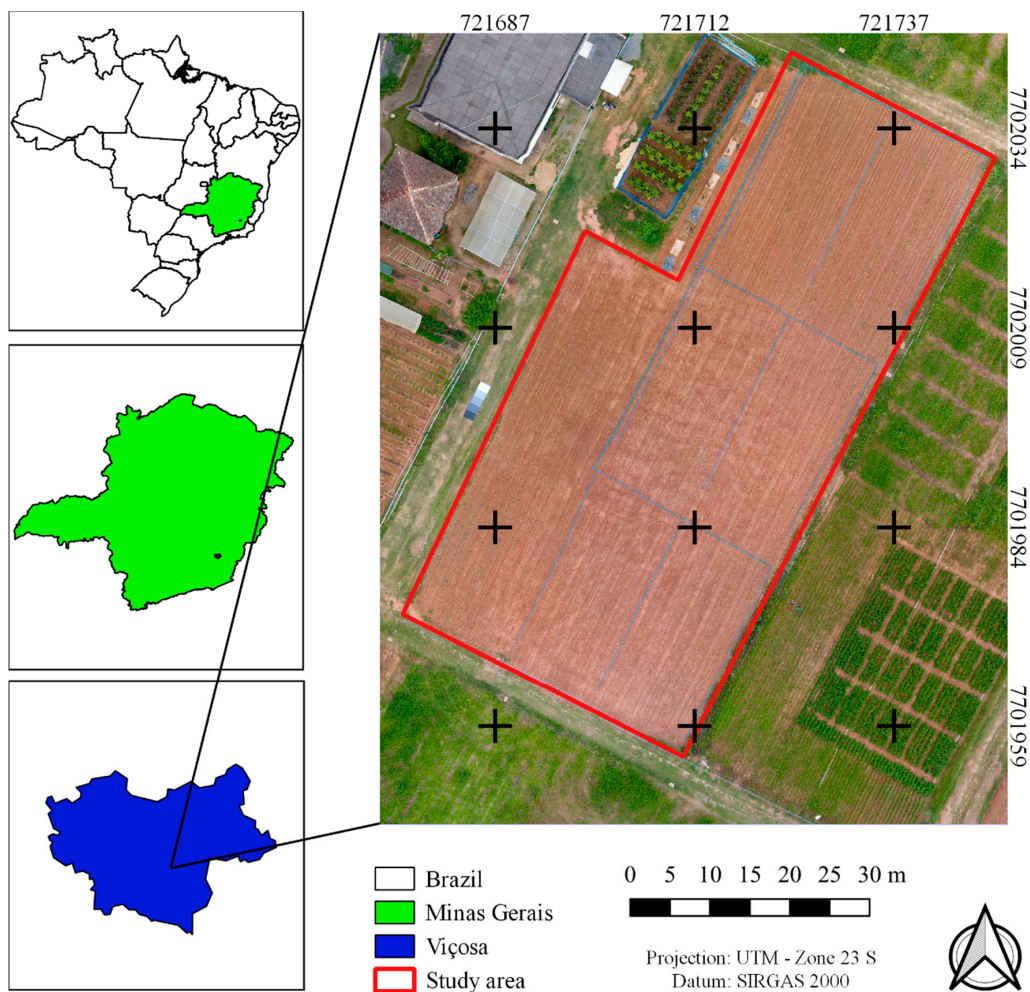


Figure 1. Location of the study area in relation to the municipality of Viçosa, Minas Gerais state, and Brazil.

2.2. Crop Planting and Management

Maize (*Zea mays* L.) was sown on 15 October 2018, with a spacing of 0.28 m between plants and 0.50 m between rows. Seedling emergence began on 20 October 2018. At 25 days after emergence (DAE), chemical control of weeds was performed using the active ingredient glyphosate at a dose of 0.89 kg ha⁻¹. Two fertilizations were performed: one involved sowing with 300 kg ha⁻¹ of the NPK formulation 8:28:16, and the other involved sowing at 38 DAE with nitrogen fertilization at the recommended dose of 300 kg ha⁻¹ using urea as the source.

2.3. Data Acquisition

2.3.1. Field Data

In total, 54 maize plants were collected at 46 (18 plants), 52 (22 plants), and 59 (14 plants) DAE to quantify the aboveground dry biomass (AGB). Different dates were used for collection to follow the temporal variability of the crop; as the maize develops, until it reaches antithesis, the vegetation index also tends to increase. In this way, the sensor was able to identify the spatial and temporal variability. The collections were carried out randomly between plants, as well as between planting rows, avoiding the collection of two nearby plants to avoid the influence of the leaf of one plant on the other, which would be captured by the RGRNIR sensor. After collection, the plants were separately placed in paper bags and dried in a forced-air circulation oven at a temperature of 70 °C for 72 h. After this period, the samples were removed from the oven, and the plants were weighed. Each collected plant was georeferenced with a Global Navigation Satellite System (GNSS) RActual-Time kinematic (RTK) Topomap T10 receiver. This receiver was used due to its high accuracy and to determine the exact location of each plant collected in the field.

2.3.2. Aerial Data

Aerial imaging started from 03 DAE and ended at 61 DAE (Table 1), always at 10 h (UTC/GMT-3). The imaging ended at 61 DAE because of the technical conditions of the device.

Table 1. Image acquisition dates and weather conditions at the time of imaging.

Date	DAE	Growth Stages	T	RH	V _w	R _s	ET _o	P _d	P _{d-1}	P _{bi}
			(°C)	(%)	(m s ⁻¹)	(MJ m ⁻² d ⁻¹)	(mm)	(mm)	(mm)	(mm)
10/22/2018	3	V2	19.65	71.50	2.70	16.42	3.41	0.00	0.00	21.2
10/31/2018	12	V3	23.95	71.00	2.50	17.53	3.83	0.00	1.60	42.6
11/02/2018	14	V4	24.4	73.50	1.30	22.46	4.38	0.20	13.20	13.4
11/07/2018	19	V5	24.25	67.00	2.00	14.88	3.29	0.00	0.200	32
11/12/2018	24	V6	24.75	67.50	1.90	20.25	4.34	0.00	0.00	67.6
11/15/2018	27	V7	24.6	73.00	3.50	18.56	4.31	7.00	0.00	7.00
11/23/2018	35	V8	22.9	71.00	3.30	17.10	4.02	0.00	0.00	139.8
11/28/2018	40	V10	22.95	70.50	1.10	24.38	4.73	0.20	10.20	13.8
11/30/2018	42	V12	24.25	68.50	3.20	23.76	5.05	5.00	0.00	5.00
12/04/2018	46	V12	22.75	74.00	0.90	14.67	3.15	0.00	3.40	29.4
12/10/2018	52	V13	19.8	80.50	0.20	15.07	3.19	0.20	1.80	64.2
12/12/2018	54	V14	24.15	67.50	2.00	26.74	5.49	0.00	0.00	0.00
12/14/2018	56	V14	25.35	63.50	2.50	29.65	6.07	0.00	0.00	0.00
12/17/2018	59	VT	25.20	66.50	3.00	28.70	5.95	0.00	0.00	0.00
12/19/2018	61	VT	27.75	60.50	2.50	27.05	5.8	0.00	0.00	0.00

DAE = Days after emergence; T = Average air temperature; RH = Average relative humidity; V_w = Average wind velocity; R_s = Incident solar radiation; ET_o = Reference evapotranspiration; P_d = Precipitation of the day; P_{d-1} = Precipitation of previous day; P_{bi} = Precipitation between imaging events.

During the imaging period, an RGNIR sensor onboard an unmanned aerial vehicle (UAV) was used to capture 15 sets of images (Table 1). The UAV used was a DJI Phantom 4 manufactured by DJI

Innovations (Figure 2). Phantom line drones are multirotor vehicles [26] with a flight autonomy of approximately 30 min.

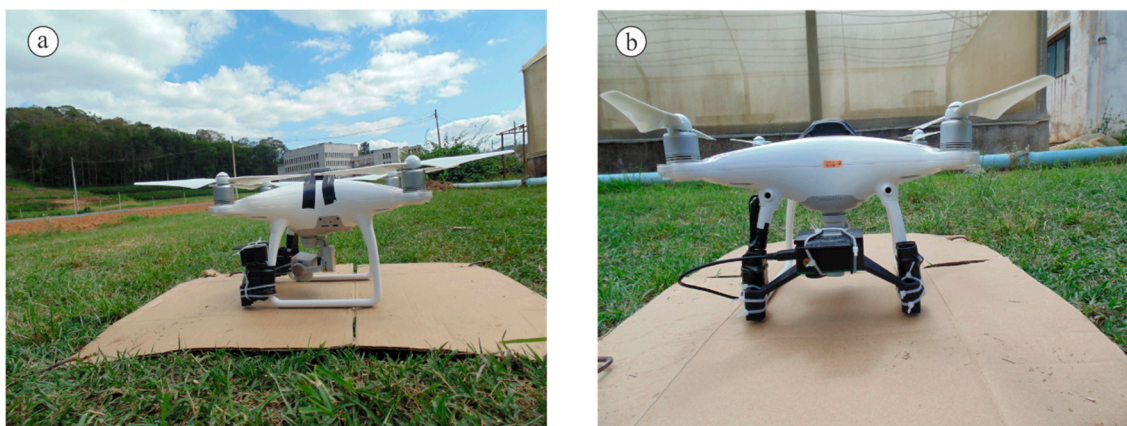


Figure 2. Unmanned aerial vehicle (UAV) used for conducting the study: (a) lateral view of the aircraft; (b) front view of the aircraft highlighting the Mapir Survey 3 sensor.

The sensor (Figure 2b) was a Survey 3 manufactured by the Mapir company. According to the manufacturer, this sensor has three filters that differentiate between the red, green, and near-infrared wavelengths. The wavelength ranges for the respective filters are 640–680, 525–575, and 820–880 nm, respectively [27]. The sensor can capture images at a resolution of 12 Megapixels (4000×3000 pixels) and with adjustable time intervals (in the present study, we used 2 s). These images were stored automatically on a micro memory card in the JPEG format with an 8-bit radiometric resolution.

For the images to always have the same pattern of capture (to avoid interfering with the results), flight planning was elaborated using the DroneDeploy application. Flight planning was set to an altitude of 50 m with a front overlap of 85%, a side overlap of 75%, and a velocity fixed at 3 m s^{-1} . The time spent by the UAV flying in the study area was approximately 3 min. After acquiring the image sets, the images were mosaiced. This process was carried out in the software Agisoft PhotoScan, thereby generating a file in the GeoTIF format with three bands (Red, Green and NIR). The images exported from this software had pixels with a spatial resolution of 0.025 m, which were aggregated to 0.5 m for optimized processing. For the field information to be estimated by the sensor, it was necessary to perform the geometric correction and digital number conversion using the physical values of reflectance to allow for the subsequent calculation of the vegetation indices.

2.4. Data Processing

2.4.1. Geometric Correction

The MAPIR survey 3 Sensor uses a GNSS receiver that allows one to capture the georeferenced images. However, the receiver has low accuracy that generates random errors in each image, thus requiring accurate georeferencing. For this purpose, eight wooden pickets were installed in the area designated for the experiment, and their coordinates were obtained by a GNSS RTK Topomap T10 receiver. These pickets served as a control point for georeferencing. Geometric correction was performed in the images after the mosaicking process.

2.4.2. Conversion from Digital Numbers to Physical Values

The sensor onboard the UAV provides image values using digital numbers (DNs), which need to be converted to physical values of reflectance. For this process, five low-cost panels at different grayscales (black; dark grey; intermediate grey; light grey; and white) were used. These panels were made of artificial Napa, a material whose composition is based on PVC, with the textile portion made

from polyester. These panels had an area of 1.5 m² each and were placed next to the study area on all flights carried out. The reflectance of each panel was determined in the laboratory using a spectroradiometer. With the aid of the QGIS[®] 2.18 software [28], the mosaiced images were cut based on the area of each panel. Subsequently, the average DNs of the red and infrared bands corresponding to each panel were extracted, and a regression was used to determine an equation of conversion between the DNs of the panels quantified by the MAPIR sensor and their average values of reflectance obtained by the spectroradiometer. This procedure was performed for each image mosaic (i.e., on each imaging occasion).

To improve the computational performance of image processing, pixels of the images were aggregated from 0.025 to 0.5 m. In this way, the images were reduced from 4,100,000 to 10,400 pixels.

2.4.3. Vegetation Indices (VI)

To analyze crop behavior during the crop cycle and apply models of evapotranspiration to the maize crop, the Normalized Difference Vegetation Index (NDVI) developed by Rouse et al. (1974) [29] and the Soil-Adjusted Vegetation Index (SAVI) developed by Huete (1988) [30] were used. These indices were obtained according to Equations (1) and (2), respectively,

$$\text{NDVI} = \frac{\rho_{\text{NIR}} - \rho_{\text{R}}}{\rho_{\text{NIR}} + \rho_{\text{R}}} \quad (1)$$

$$\text{SAVI} = \frac{\rho_{\text{NIR}} - \rho_{\text{R}}}{\rho_{\text{NIR}} + \rho_{\text{R}} + L} * (1 + L) \quad (2)$$

where ρ_{NIR} is the near-infrared reflectance, ρ_{R} is the red reflectance, and L is the soil adjustment factor. This factor varies according to the canopy density, and values from 0.25 to 1.0 can be adopted. However, the present study adopted 0.5, as recommended by Huete (1998) [30], and applied the general approach by García and Pérez (2016) [31] and Gilabert et al. (2002) [32], and the specific approach for maize crops by Zhang et al. (2019) [33].

2.4.4. Actual Crop Evapotranspiration from VI

After estimating the indices, the actual crop evapotranspiration (ET_a) was calculated. ET_a is the sum of the actual transpiration (T_a) and evaporation (E). The actual transpiration (Equation (3)) is a biophysical process involving water loss through the stomata present in the leaves after being involved in the physiological processes of the plant [34] while considering the soil moisture conditions

$$T_a = K_{cb} * K_s * ET_o \quad (3)$$

where K_{cb} is the basal crop coefficient, K_s is the stress coefficient, and ET_o is the reference evapotranspiration calculated from the meteorological data by the Food and Agriculture Organization (FAO)-56 method [16].

In turn, evaporation (Equation (4)) is a physical process of water loss from the soil or the surface of plants, as water transitions from a liquid form to vapor [16]

$$E = K_e * ET_o \quad (4)$$

where K_e is the evaporation coefficient.

K_{cb} Estimated by the VI

According to Choudhury et al. (1994) [35], there is an exponential relationship between the transpiration coefficient (T_c), shown in Equation (6), and the leaf area index (LAI). Thus, when the LAI is maximal, the crop will have a higher coefficient of transpiration. T_c is described as the ratio of transpiration under stress-free conditions to the maximum crop evapotranspiration when the vegetation

fully covers the soil (that is, under higher values of LAI). Thus, K_{cb} is given by the product of the maximum value of K_{cb} (K_{cbmax}) (the tabulated value [16]) and the coefficient of transpiration (Equation (5))

$$K_{cb} = K_{cbmax} * T_c \quad (5)$$

When no saturation occurs, the maximum value of LAI coincides with the maximum value of VI [35]. Choudhury et al. (1994) [35] replaced LAI with VI to estimate T_c (Equation (6))

$$T_c = 1 - \left(\frac{VI_{max} - VI}{VI_{max} - VI_{min}} \right)^n \quad (6)$$

where n corresponds to the K/K' ratio; K is a coefficient related to the leaf architecture of the crop, varying from 0.5 to 0.7; and K' is a coefficient that varies from 0.5 to 0.7 and from 0.8 to 1.3 when the vegetation indices used are SAVI and NDVI, respectively [35].

Replacing T_c in Equation (5) with Equation (6) yields K_{cb} from the VI (Equation (7))

$$K_{cb} = K_{cbmax} \left[1 - \left(\frac{VI_{max} - VI}{VI_{max} - VI_{min}} \right)^n \right] \quad (7)$$

Equation (7) is a generalized model used to determine the K_{cb} of the crop from the VI. The K_{cbmax} adopted for the maize crop was 1.15 [16].

In the present study, the VIs of Equations (1) and (2) were used to determine the K_{cb} of maize throughout its growth. For NDVI, it was only necessary to replace the VI of Equation (7) with the NDVI values, assuming the mean value between coefficients K and K' . For SAVI, the VI parameters of the equation above were replaced; however, according to Choudhury et al. (1994) [35], the ratio between K and K' is equal to 1.

Evaporation Coefficient (K_e)

To quantify the K_e , it was necessary to determine the daily water balance in the soil over the 61 days of crop monitoring. In the study area, the soil was collected to measure the field capacity on a volumetric basis (θ_{FC}), the wilting point on a volumetric basis (θ_{WP}), and the soil bulk density (d_s). The soil of the study area had a θ_{FC} of $0.33 \text{ m}^3 \text{ m}^{-3}$, a θ_{WP} of $0.21 \text{ m}^3 \text{ m}^{-3}$, and a density of 1.20 kg m^{-3} . θ_{FC} and θ_{WP} were used to calculate the maximum water depth that could be evaporated, as suggested by Allen et al. (1998) [16], using a 0.10 m layer of soil subject to evaporation. The entire water balance procedure was carried out strictly as described in Bulletin 56 published by FAO [16].

Stress Coefficient (K_s)

K_s was quantified via the daily soil water balance using Equation (8) [16]

$$K_s = \frac{TAW - D_r}{TAW - RAW} = \frac{TAW - D_r}{(1 - p) RAW} \quad (8)$$

where TAW is the total available soil water in the root zone (mm), D_r is the moisture depletion, RAW is the readily available water in the root zone, and p is the fraction of TAW that the plant can extract from the root zone without undergoing water stress.

TAW is calculated based on the daily rooting depth of the crop (Z_r) along with θ_{FC} and θ_{WP} (Equation (9))

$$TAW = 1000(\theta_{FC} - \theta_{WP})Z_r \quad (9)$$

RAW was calculated by Equation (10)

$$RAW = pTAW \quad (10)$$

According to FAO Bulletin 56 [16], the p for a maize crop is 0.55 when the crop potential ET (ET_{pc}) is equal to 5 mm d^{-1} . When the ET_{pc} diverges from 5 mm d^{-1} , Equation (11) is used for correction

$$p = 0.55 + 0.04(5 - ET_{pc}) \quad (11)$$

After completing all the processes above, the actual transpiration and evapotranspiration of the crop were determined.

2.4.5. Estimation of Aboveground Dry Biomass

The aboveground dry biomass (AGB) was calculated using the model developed by Monteith (1972) [36] according to Equation (12), which quantifies the daily increase in the dry biomass of the crop based on the water and radiation parameters

$$AGB = \varepsilon_{max} \cdot E_f \cdot APAR \cdot 0.864 \quad (12)$$

where AGB is the aboveground dry biomass in $\text{kg ha}^{-1} \text{ d}^{-1}$; ε_{max} is the maximum radiation use efficiency, which is equal to 3.5 g MJ^{-1} for maize [19]; E_f is the evaporative fraction; APAR is the absorbed photosynthetically active radiation (W m^{-2}); and 0.864 is the factor for unit conversion.

The evaporative fraction was replaced by the ratio between the actual crop evapotranspiration and the reference evapotranspiration used by some authors [37,38], which was also adopted in the present study.

The APAR was obtained by the product between the NDVI and incident solar radiation (R_s) [39–41], according to Equation (13)

$$APAR = (1.26 \cdot NDVI - 0.16) \cdot (0.48 \cdot R_s) \quad (13)$$

To statistically compare the aboveground dry biomass estimated by the models and the aboveground dry biomass observed in the field, the geographic coordinates of each plant collected were used to establish a 1 m radius from the georeferenced point and generate a representative circular area of 3.14 m^2 for each plant collected. This area provided the average biomass increase on each day of the imaging until plant collection. Subsequently, the values of daily biomass were integrated with time to obtain the value of the dry biomass accumulated until the day of the collection.

2.5. Validation of Estimated Aboveground Dry Biomass

Since biomass is a parameter measured in the field, validation using measurements of dry biomass was performed to assess the reliability of the models for actual crop evapotranspiration (ET_a) estimated by the VI because it was not possible to measure ET_a in the field during the experimental period.

For statistical comparisons between the estimated and observed AGB, the statistics presented in Equations (14)–(17) were applied to quantify the relationships and the errors between the biomass measured in the field and the biomass estimated by the images of the UAV

$$R^2 = \frac{\left[\sum_{i=1}^n (P_i - \bar{P})(O_i - \bar{O}) \right]^2}{\left[\sum_{i=1}^n (P_i - \bar{P})^2 \right] \left[\sum_{i=1}^n (O_i - \bar{O})^2 \right]} \quad (14)$$

$$RMSE = \sqrt{\frac{\sum_{i=1}^n (P_i - O_i)^2}{n}} \quad (15)$$

$$MAE = \frac{1}{n} \sum_{i=1}^n |P_i - O_i| \quad (16)$$

$$MBE = \frac{1}{n} \sum_{i=1}^n (P_i - O_i) \quad (17)$$

where P_i is the value predicted by the model, O_i is the observed value, \bar{P} is the average value obtained by the model, \bar{O} is the average value observed, and n is the sample number.

3. Results and Discussion

3.1. K_{cb} Derived from the VIs

The mean values of the vegetation indices (VIs) NDVI and SAVI can be visualized in Figure 3. The VIs were observed to increase over time following plant growth.

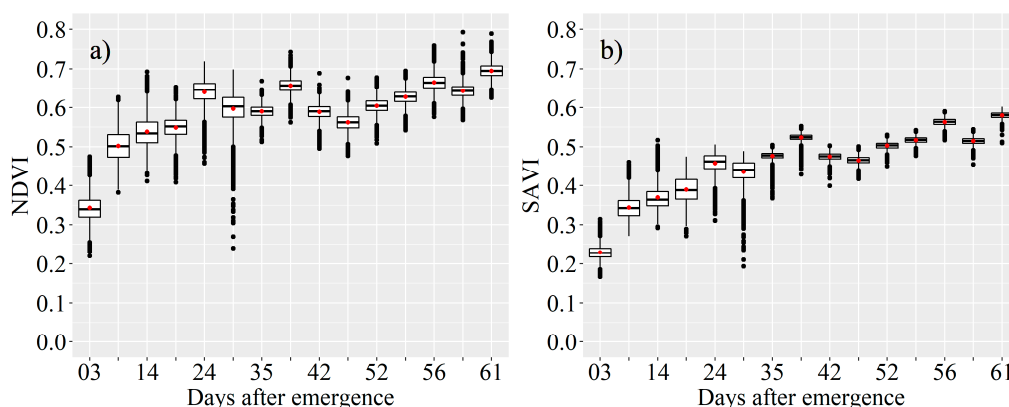


Figure 3. Descriptive statistics of the temporal and spatial variability of maize crops by Normalized Difference Vegetation Index (NDVI) (a) and Soil-Adjusted Vegetation Index (SAVI) (b).

The NDVI values are higher than SAVI values because of the L coefficient used for soil brightness attenuation present in the methodology of the latter. For both indices, greater spatial variability was observed from 03 to 27 DAE, as illustrated by the greater interval between the first and third quartiles of the boxplots. This situation occurred because of the high weed infestation in the experimental area since the crop does not yet fully cover the cultivated area. Ten days after chemical control, this variability was reduced, and only maize plants were present in the area. For NDVI, the maximum recorded value was 0.69, and for SAVI, the maximum value was 0.58—both at 61 DAE. Zhang et al. (2019) [33], using a MicaSense Red Edge sensor onboard a UAV, found maximum values of NDVI and SAVI for a maize crop at 75 DAE, equal to 0.85 and 0.65, respectively. For NDVI, Toureiro et al. (2017) [42] found a maximum value of 0.80 at 85 DAS (days after sowing) for a maize crop using images from Landsat 5. Taghvaeian et al. (2012) [43], using terrestrial sensors, found a maximum value of 0.69 for SAVI, noting that maize plants fully covered the soil.

Figure 4 presents the mean values of K_{cb} , K_e , dual K_c , and K_s for the maize crop on each day of the image.

As observed in Figure 3, the VI tends to increase with crop growth. Thus, the K_{cb} values derived from these indices also tend to increase (Figure 4a) following an increase in the VIs. However, a greater discrepancy is observed with the K_{cb} determined by the empirical model of NDVI. This result may be related to the coefficient “ n ” applied to the model, which determines the K_{cb} via the NDVI proposed by Choudhury et al. (1994) [35], whereas SAVI does not use this coefficient [44].

Studies using K_{cb} derived from NDVI have demonstrated a good linear relationship, with a coefficient of determination above 0.80 between K_{cb} and NDVI [12,42]. Likewise, the present study found linearity between these two parameters, with an R^2 of 0.81, whereas SAVI and its relationship with K_{cb} yielded an R^2 of 0.99. This difference between the two indices is related to the aforementioned coefficient “ n ”.

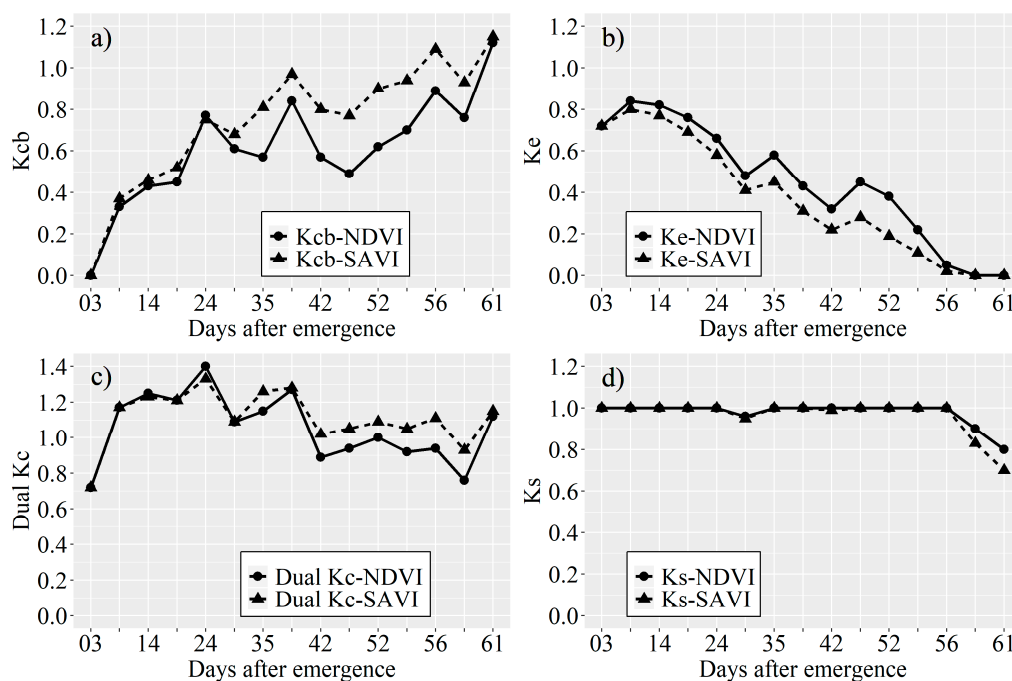


Figure 4. Mean values of K_{cb} (a), K_e (b), dual K_c (c), and K_s (d) for the maize crop 61 days after emergence.

By using the NDVI index to estimate K_{cb} , a saturation of the vegetation index may occur, especially for plants with a C4 metabolism. This means that the plant will continue to develop, but the K_{cb} estimated by the NDVI will remain stable at a maximum limit. However, according to Duchemin et al. [44], the impact of NDVI saturation is not critical for the estimation of transpiration. The SAVI index, on the other hand, due to the L coefficient of soil brightness attenuation, does not show saturation and may be more appropriate for reducing errors in the estimation of K_{cb} and subsequent transpiration.

Contrary to the K_{cb} value (Figure 4a), K_e (Figure 4b) tends to decrease as the crop grows and develops. This is a normal condition, as the effect of this coefficient is reduced with an increase in vegetation cover. The expansion of leaf area intercepts solar radiation, which can reach the ground, reducing the latent heat of vaporization. Consequently, with less energy interacting with the moist soil, there will be less evaporation of water from the soil. Another factor affecting the value of K_e is the soil moisture condition, as moister and more exposed soil has greater potential for evaporation [45]. Figure 4b shows that the reduction in K_e is not constant, with variations in the values caused mainly by precipitation (Table 1). As observed for K_{cb} , the values of K_e differ in the same image based on the parameter's calculation, as proposed by the FAO Bulletin 56 [16], which takes into account the values of K_{cb} .

Figure 4c presents the value of the dual K_c obtained by the sum of K_{cb} and K_e . Throughout the crop cycle, the dual K_c values were high, almost always close to 1.00. At the beginning of the cycle, the dual K_c values were influenced mainly by the high value of K_e due to the availability of water in the soil and decreased with maize growth. In Figure 4c, it is possible to observe that some values of dual K_c exceed 1.20. Theoretically, this should not happen because, when calculating K_e , the value of 1.20 is adopted as the maximum K_c allowed for the maize crop [16]. Thus, until the moment that K_e exerts influence on the dual K_c , the latter's value should not exceed 1.20, and, when K_e ceases to exert influence, this value should not exceed 1.15 (maximum K_{cb} for maize). However, due to the presence of weeds and excess moisture in the evaporating layer, higher values of K_{cb} occurred at the beginning of the cycle.

During the monitoring, a total precipitation of 436.00 mm (Table 1) was recorded, with occurrence at least once a week until 52 DAE. From that day until 61 DAE, there was no record of precipitation.

Thus, the soil was expected to remain close to field capacity until 52 DAE. Figure 4d presents the stress coefficient (K_s) in the experimental area, where mild stress was observed at 27 DAE due to low precipitation (7 mm) over an interval of 3 days. K_s decreased slightly after 56 DAE and more sharply at 59 and 61 DAE. As there was a drought period from 52 DAE, the water present in the effective root system zone was demanded by the atmosphere through the processes of evaporation and transpiration, which, consequently, reduced the water content available for the crop (i.e., by increasing moisture depletion in this zone and causing the plant to spend more energy to remove the water chemically bound to the soil). The SAVI model used to determine K_{cb} was more sensitive to water stress because this model tends to have a higher basal coefficient, thereby influencing the greater potential transpiration of the crop.

3.2. Actual Transpiration and Evapotranspiration of the Maize Crop

The actual transpiration of the crop (T_a) is presented in Figure 5. Low values of T_a occurred at the beginning of the cycle due to the lower vegetation cover (i.e., the smaller the photosynthetic component, the less the transpiration).

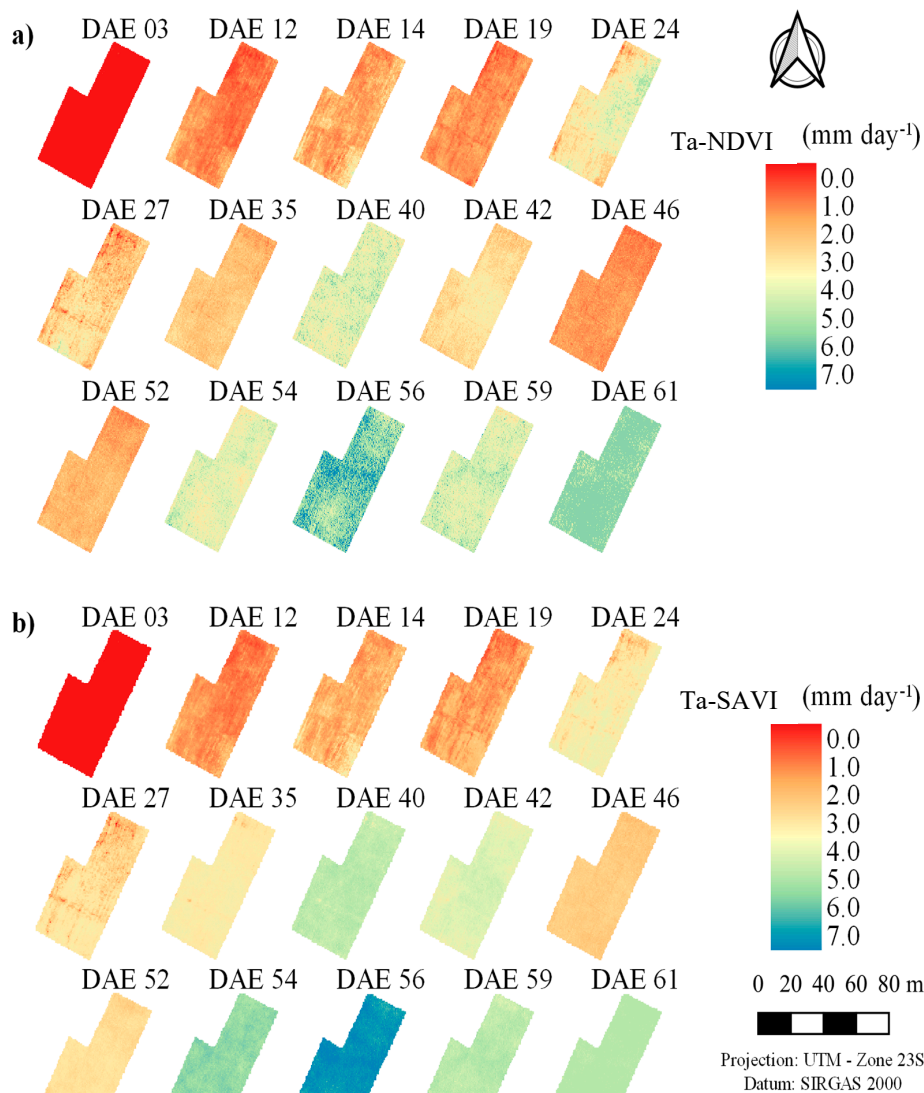


Figure 5. Actual transpiration of maize crop determined by the methodologies derived from NDVI (a) and SAVI (b).

At 14 DAE, it is possible to observe isolated areas in the image with transpiration around 3 mm caused by the incidence of weeds in the area with an ET_o of 4.58 mm (Table 1). In the images for 19 DAE, the weeds showed more advanced development than those in the previous images, but their T_a was lower due to the ET on this day (3.29 mm). At 24 DAE, there was high variability of T_a influenced by the strong weed development and high value of ET_o (4.34 mm).

After herbicide application (25 DAE), there was a reduction in the T_a rate influenced by the effects of the toxicity of the active ingredient on the weeds. Glyphosate prevents CO_2 assimilation by reducing the stomatal conductance and, consequently, the transpiration of the plants [46]. Another factor that influenced the T_a on this day was K_s (Figure 4d), which reduced the transpiration of the crop via water stress. From 35 DAE, only the maize crop prevailed in the area, so transpiration from the experimental area was influenced by both the crop and the environmental conditions during imaging. At 46 and 52 DAE, there was a sudden reduction in T_a . This occurrence was attributed to the low radiation on these days, which reduced the photosynthesis and transpiration rates along with the low estimated value of ET_o (Table 1). The image for day 56 was strongly influenced by ET_o (Table 1) and by the absence of water stress, $K_s = 1.00$ (Figure 4d). Thus, at 56 DAE, the crop had higher T_a . For days 59 and 61, crop transpiration was limited by the water stress ($K_s < 1$) caused by drought. Thus, although the crop had high vegetative vigor, its values of ET_o were close to 6 mm (Table 1), so the T_a was lower than 5.5 mm on average.

The T_a determined by the empirical model of K_{cb} derived from the NDVI showed greater spatial variability than the empirical model of K_{cb} derived from SAVI. This phenomenon can be observed in Figures 5 and 6. In Figure 6a, a greater interval than that in Figure 6b can be clearly observed between the first and third quartiles. The discrepancy between the models is related to the aforementioned coefficient “n”.

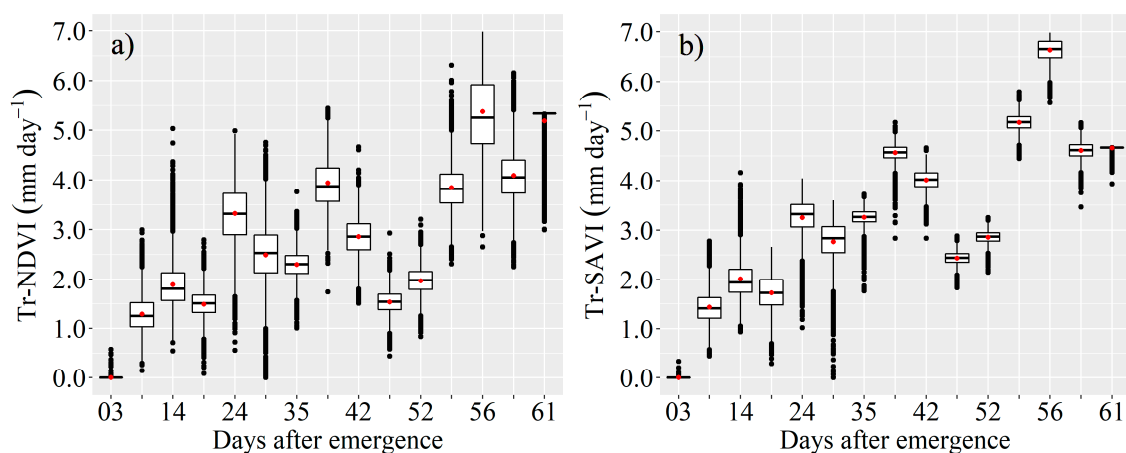


Figure 6. Descriptive statistics of the actual transpiration of maize crop by the models derived from the NDVI (a) and SAVI (b).

The transpiration of the crop facilitates the accumulation of AGB, since the efflux of water through the stomatal opening occurs simultaneously with the influx of CO_2 , and the latter is related to the photosynthetic process [34,47]. Past studies demonstrated that an increase in CO_2 entering into the maize plant, up to a certain limit, positively impacts the increase in its biomass (with water available in the soil) [17,48,49]. Thus, the transpiration model most strongly related to AGB has greater potential for predicting transpiration.

Figure 7 presents the relationship between the AGB of maize plants collected in the field and the accumulation of the actual crop transpiration for the models derived from the NDVI (Figure 7a) and SAVI (Figure 7b). This Figure shows that the empirical model based on SAVI has a higher predictive capacity than the model based on NDVI, providing an R^2 of 0.74 for the maize biomass. Campos et al. (2018b) [50], using values of K_{cb} derived from SAVI and corrected by water and thermal

stress coefficients, recorded an R^2 of 0.94 for the biomass of the same crop in rainfed areas and 0.96 in irrigated areas, albeit using satellite images, unlike the present study, which used low-cost sensors. Twohey et al. (2019) [51], measuring the direct transpiration of maize in a greenhouse, found an R^2 of 0.92 for the maize's biomass. The predictive capacity of transpiration using a low-cost sensor onboard a UAV is important for the agricultural monitoring of crop water conditions in areas with low investment capital where it is not possible to perform orbital imaging.

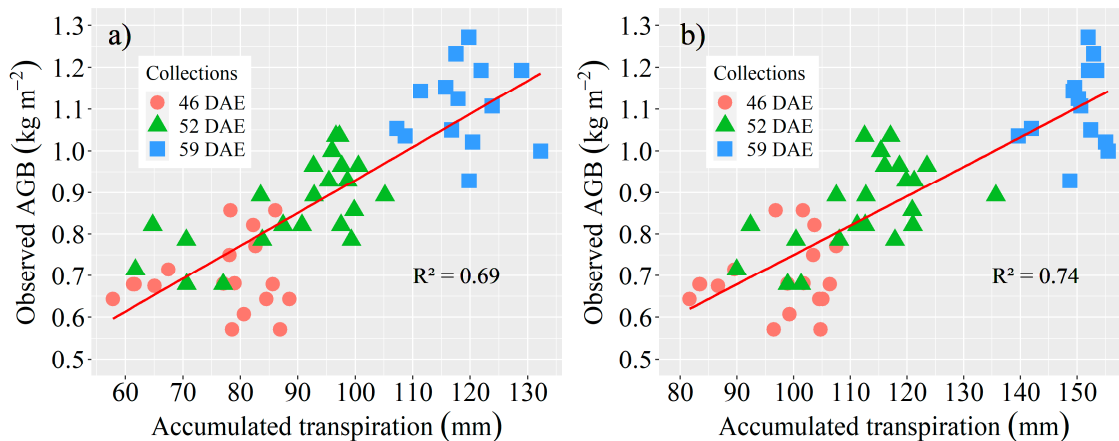


Figure 7. Linear regression between the accumulated actual transpiration (iT_a) of the maize crop (with its biomass) using the models derived from the NDVI (a) and SAVI (b).

The actual evapotranspiration of the crop (ET_a) obtained by the coefficients of the plant, soil, and ET_o is shown in Figure 8. The ET_a is high at the beginning of the crop cycle, unlike the values of T_r , especially when the soil is not protected from the vegetation cover. These higher values of ET_a are due to the evaporation of water present in the soil. This indicates that transpiration was low during these days and that evaporation from the diffusion of water vapor present in the evaporative layer was high. These situations were also observed by Rosa et al. (2016) [45] when studying dual K_c in a maize crop under field conditions. The same behavior of spatial and temporal variability observed for T_a was also observed for ET_a . The influence of the evaporative component occurs until 56 DAE (Figure 4b). From this day, the water demand of the area is due to the transpiration component.

Figure 9 illustrates the influence of K_e on the water demand of the crop. Here, the average of the boxplots starts above 2 mm, contrary to Figure 6.

The methodology based on dual K_c normally tends to present higher values of evapotranspiration at the beginning of the crop cycle because it considers the quantification of two isolated coefficients that are summed [45]. Conversely, when the water content is quantified using a single K_c , the estimate of water demand in the initial stages of the crop tends to be lower, since this K_c represents the mean value between the evaporation of soil water and the transpiration of the crop [52].

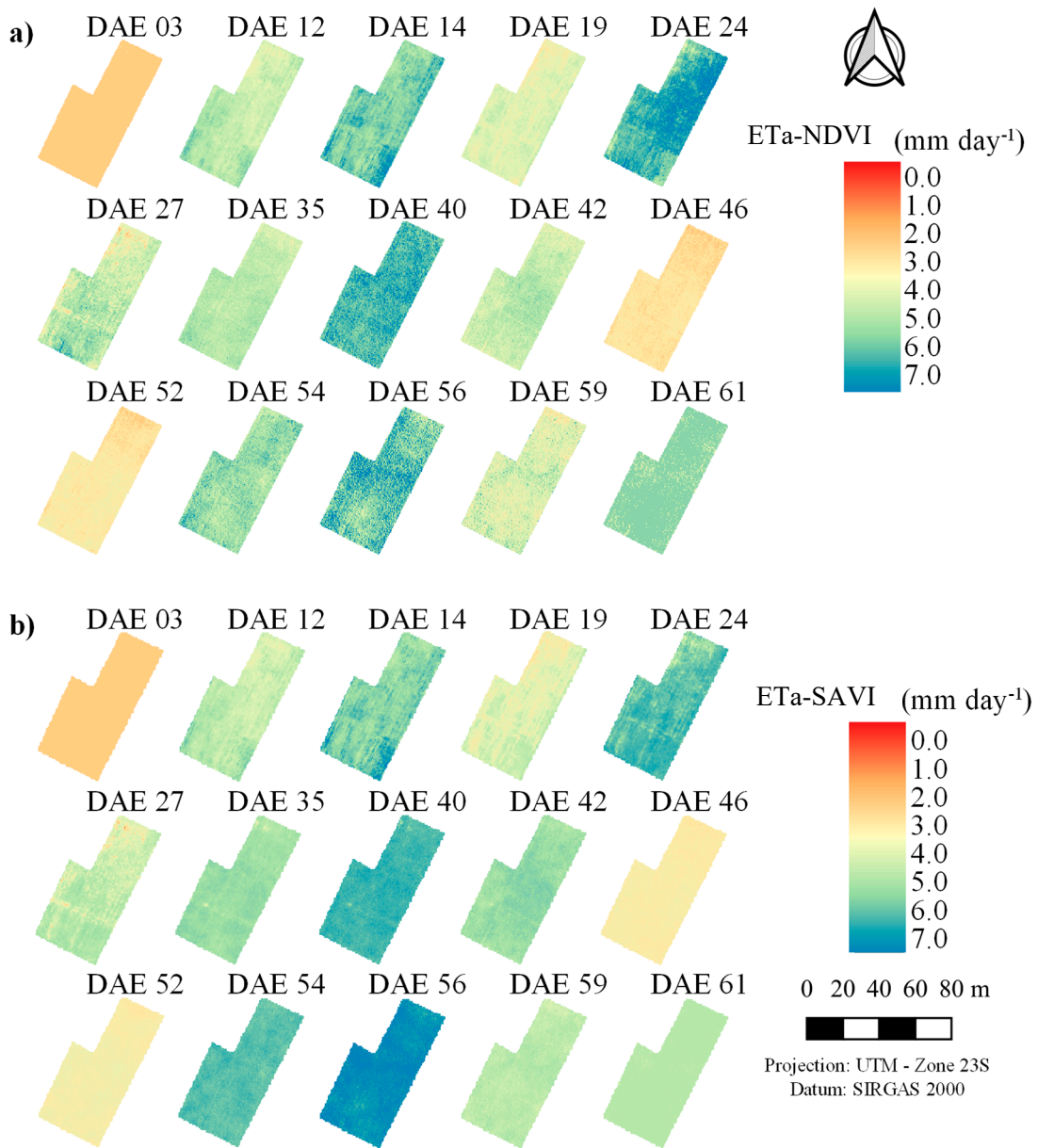


Figure 8. Actual evapotranspiration of the crop using the empirical models derived from the NDVI (a) and SAVI (b).

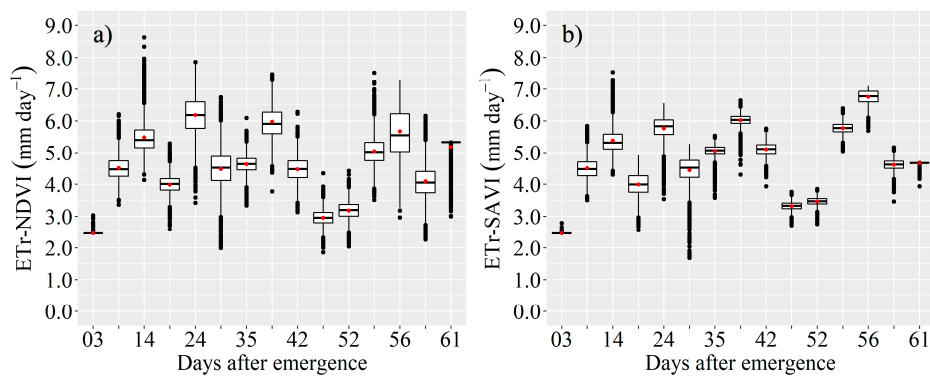


Figure 9. Descriptive statistics of actual evapotranspiration of the crop using the models derived from the NDVI (a) and SAVI (b).

3.3. Estimation of AGB

Figure 10 shows the spatial and temporal variation of the daily increase in aboveground dry biomass (AGB) using the evaporative fraction derived from the NDVI and SAVI. Until 24 DAE, the daily increase was promoted by both the crop (still at the beginning of its growth) and the weeds present in the area, as discussed earlier. After day 27, the largest daily increases occurred at 40 and 56 DAE, and the lowest increases occurred at 46 and 52 DAE for both models. On days 40 and 56, the daily incident solar radiation was equivalent to 23.38 and 29.25 MJ m⁻² d⁻¹ (Table 1), respectively. At 46 and 52 DAE, the radiation was 14.67 and 15.07 MJ m⁻² d⁻¹ (Table 1), respectively. Thus, radiation promoted gains in the daily increase in biomass.

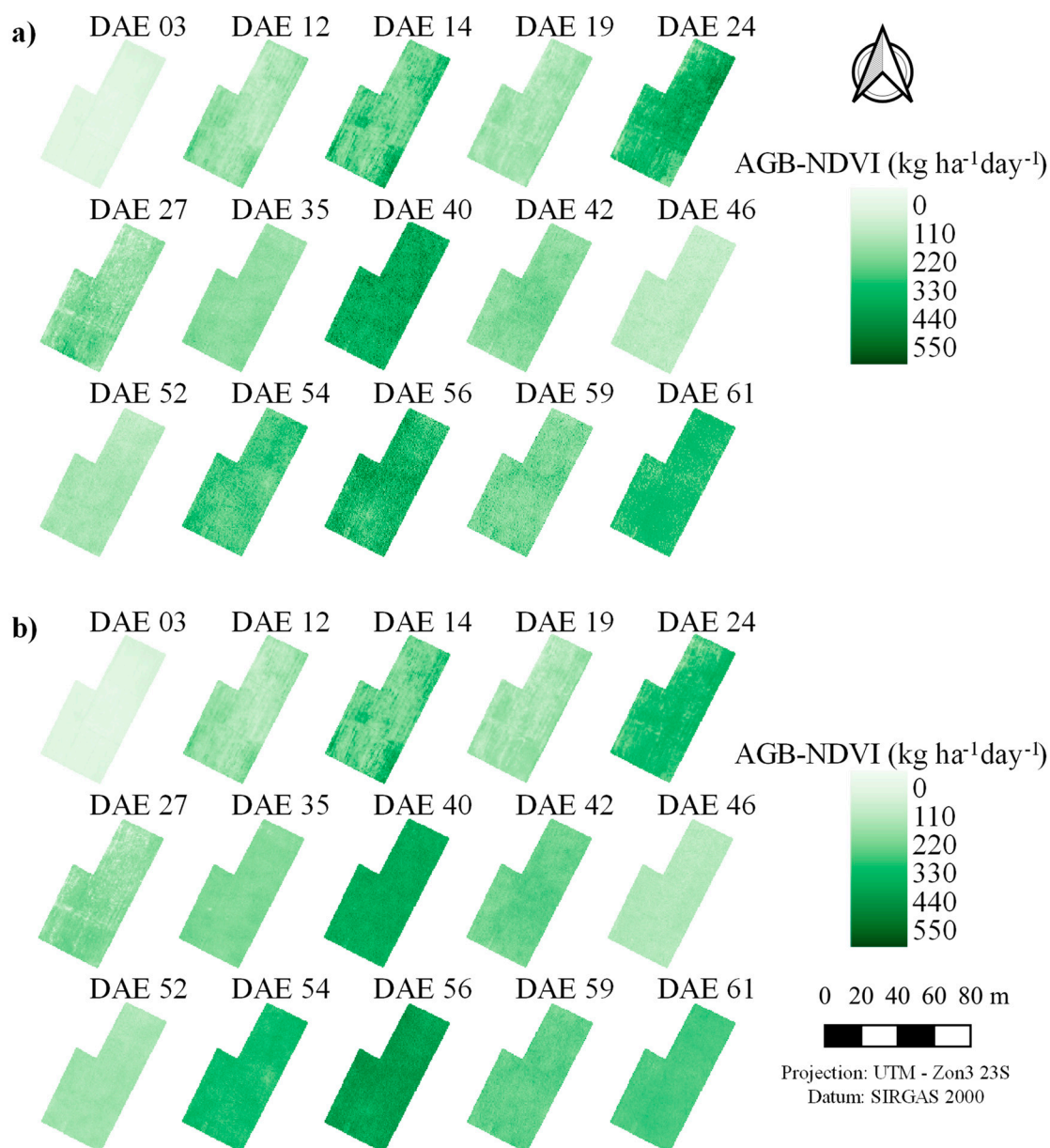


Figure 10. Spatial and temporal variability of the daily increase in aboveground dry biomass derived from the NDVI (a) and SAVI (b).

Solar radiation is the parameter used to calculate the photosynthetically active radiation established in Equation (13). Thus, the higher the radiation is, the more the biomass will increase. Solar radiation stimulates the photosynthesis, formation, and development of plant organs, as well as biomass

and grain yield [53]. Thus, the larger the amount of radiation reaching the crop is, the higher the photosynthetic rate and increase in biomass will be. Another factor that influences biomass production when using the model in Equation (12) is the evaporative fraction, which is the ratio between the actual evapotranspiration of the crop and the reference evapotranspiration. In the images for 59 and 61 DAE, the stress coefficient was below 1 (Figure 4d), thereby reducing the evaporative fraction and, consequently, reducing the daily increase in biomass. Some recent studies have shown the negative influence of water stress on maize biomass [54–57]. However, this premise has already been scientifically consolidated.

Figure 11 presents the same behavior of variability for ET_a (Figure 8). The first and third quartiles of Figure 11a are higher than those of Figure 11b because the input evaporative fraction in the model comes from ET_a .

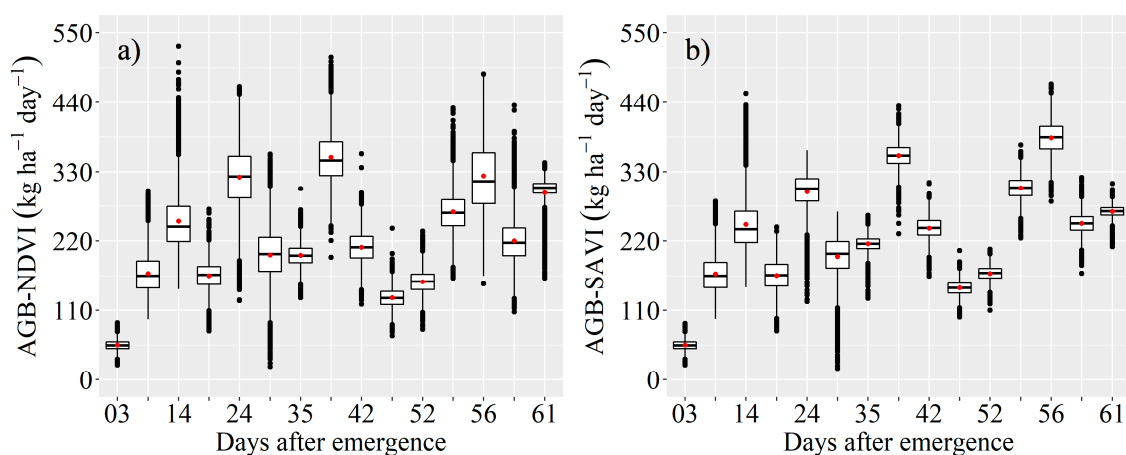


Figure 11. Descriptive statistics for the daily increase in aboveground dry biomass using the models derived from the NDVI (a) and SAVI (b).

The statistical metrics can be visualized in Figure 12 along with a regression in the estimated accumulated AGB versus the observed AGB.

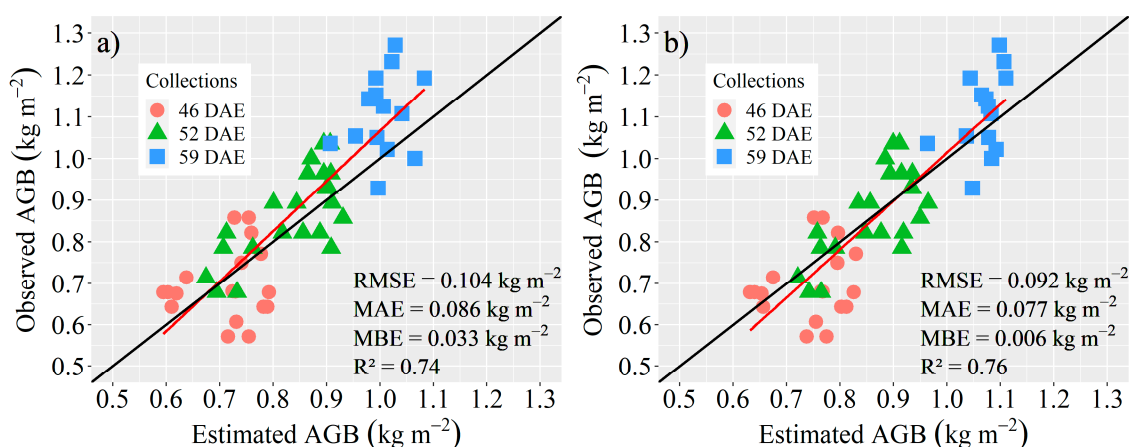


Figure 12. Statistical evaluation between the biomass estimated by the models derived from the NDVI (a) and SAVI (b) and the biomass measured in the field.

The AGB estimated using the evaporative fraction derived from the NDVI tends to overestimate the true values by 0.033 kg m^{-2} on average, with an RMSE of 0.104 kg m^{-2} and an R^2 of 0.74 (Figure 12a). The estimation of AGB using the evaporative fraction derived from the SAVI model tends to overestimate the true values, on average, by 0.006 kg m^{-2} , with an RMSE of 0.092 kg m^{-2} and an

R^2 of 0.76 (Figure 12b). Thus, using a model based on SAVI to calculate the K_{cb} offers demonstrably superior performance for estimating the AGB.

In general terms, using an RGNIR sensor to quantify the evaporative fraction and applying the model to estimate the increase in daily biomass proved to be relatively precise. This makes the use of an RGNIR camera a viable alternative for predicting the AGB, which is extremely important for farmers who need greater spatial and predictive details for their crops.

4. Conclusions

The use of an RGNIR sensor onboard a UAV was able to identify the spatial and temporal variability of a maize crop, along with its vegetative development. This result is important because the present device has a low acquisition cost. When applying the NDVI and SAVI vegetation indices, it was possible to note disturbances in the experimental area, caused mainly by weed infestations and water stress.

The K_{cb} estimated with the RGNIR camera using empirical models based on the vegetation indices proved to be a viable alternative for water management in agricultural crops, which is of great interest in small rural properties due to the low cost and versatility of the equipment.

The actual transpiration of the crop using the K_{cb} derived from SAVI had a better correlation with the biomass collected in the field compared to the transpiration calculated by the K_{cb} derived from the NDVI.

The statistical analyses revealed that the biomass estimated using the models of the evaporative fraction derived from the vegetation indices tends to overestimate the biomass measured in the field. Estimating the biomass using the evaporative fraction derived from SAVI was more satisfactory, presenting fewer errors and a better coefficient of determination than the model derived from NDVI.

The results achieved in the present study make it possible to spatially manage water in agriculture using UAV and RGNIR sensors, thereby integrating irrigation management into the assumptions of precision irrigation.

Author Contributions: Conceptualization, R.A.d.S., R.F. and E.C.M.; methodology, R.A.d.S., R.F., E.I.F.-F., E.C.M., A.C.B.d.S. and L.P.V.; software, R.A.d.S. and R.F.; validation, R.A.d.S., R.F., E.I.F.-F. and E.C.M.; formal analysis, R.A.d.S. and R.F.; investigation, R.A.d.S. and R.F.; resources, E.I.F.-F., R.F., E.C.M. and A.C.B.d.S.; data curation, R.A.d.S.; writing—original draft preparation, R.A.d.S.; writing—review and editing, R.A.d.S., R.F., E.C.M., E.I.F.-F. and L.P.V.; visualization, R.F. and E.C.M.; supervision, E.C.M. and E.I.F.-F.; project administration, E.C.M.; funding acquisition, E.C.M. and E.I.F.-F. All authors have read and agreed to the published version of the manuscript.

Funding: This research was funded by Federal University of Viçosa—UFV and by the Coordination for the Improvement of Higher Education Personnel—CAPES grant number, grant number 88882.349495/2019-01 and finance code 001.

Conflicts of Interest: The authors declare no conflict of interest.

References

- Zheng, H.; Ying, H.; Yin, Y.; Wang, Y.; He, G.; Bian, Q.; Cui, Z.; Yang, Q. Irrigation leads to greater maize yield at higher water productivity and lower environmental costs: A global meta-analysis. *Agric. Ecosyst. Environ.* **2019**, *273*, 62–69. [CrossRef]
- Tilman, D.; Balzer, C.; Hill, J.; Befort, B.L. Global food demand and the sustainable intensification of agriculture. *Proc. Natl. Acad. Sci. USA* **2011**, *108*, 20260–20264. [CrossRef] [PubMed]
- UNESCO. Water in a Changing World: The United Nations World Water Development Report 3. 2009. Available online: http://www.unesco.org/new/fileadmin/MULTIMEDIA/HQ/SC/pdf/WWDR3_Facts_and_Figures.pdf (accessed on 19 July 2020).
- Mulla, D.J. Twenty five years of remote sensing in precision agriculture: Key advances and remaining knowledge gaps. *Biosyst. Eng.* **2013**, *114*, 358–371. [CrossRef]
- Hunt, E.R.; Daughtry, C.S.T. What good are unmanned aircraft systems for agricultural remote sensing and precision agriculture? *Int. J. Remote Sens.* **2018**, *39*, 5345–5376. [CrossRef]

6. Tunca, E.; Köksal, E.S.; Çetin, S.; Ekiz, N.M.; Balde, H. Yield and leaf area index estimations for sunflower plants using unmanned aerial vehicle images. *Environ. Monit. Assess.* **2018**, *190*, 682. [CrossRef]
7. Manfreda, S.; McCabe, M.F.; Miller, P.E.; Lucas, R.; Madrigal, V.P.; Mallinis, G.; Dor, E.B.; Helman, D.; Estes, L.; Ciraolo, G.; et al. On the use of unmanned aerial systems for environmental monitoring. *Remote Sens.* **2018**, *10*, 641. [CrossRef]
8. Maes, W.H.; Steppe, K. Perspectives for remote sensing with unmanned aerial vehicles in precision agriculture. *Trends Plant Sci.* **2019**, *24*, 152–164. [CrossRef]
9. Rabatel, G.; Gorretta, N.; Labbé, S. Getting simultaneous red and near-infrared band data from a single digital camera for plant monitoring applications: Theoretical and practical study. *Biosyst. Eng.* **2014**, *117*, 2–14. [CrossRef]
10. Gowravaram, S.; Tian, P.; Flanagan, H.; Goyer, J.; Chao, H. UAS-based multispectral remote sensing and ndvi calculation for post disaster assessment. *ICUAS 2018* **2018**, 684–691. [CrossRef]
11. Nijland, W.; de Jong, R.; de Jong, S.M.; Wulder, M.A.; Bater, C.W.; Coops, N.C. Monitoring plant condition and phenology using infrared sensitive consumer grade digital cameras. *Agric. Meteorol.* **2014**, *184*, 98–106. [CrossRef]
12. Bausch, W.C.; Neale, C.M.U. Crop coefficients derived from reflected canopy radiation—A concept. *Trans. ASAE* **1987**, *30*, 703–709. [CrossRef]
13. Er-Raki, S.; Chehbouni, A.; Guemouria, N.; Duchemin, B.; Ezzahar, J.; Hadria, R. Combining FAO-56 model and ground-based remote sensing to estimate water consumptions of wheat crops in a semi-arid region. *Agric. Water Manag.* **2007**, *87*, 41–54. [CrossRef]
14. González-Dugo, M.P.; Mateos, L. Spectral vegetation indices for benchmarking water productivity of irrigated cotton and sugarbeet crops. *Agric. Water Manag.* **2008**, *95*, 48–58. [CrossRef]
15. Campos, I.; Neale, C.M.U.; Arkebauer, T.J.; Suyker, A.E.; Gonçalves, I.Z. Water productivity and crop yield: A simplified remote sensing driven operational approach. *Agric. Meteorol.* **2018**, *249*, 501–511. [CrossRef]
16. Allen, R.G.; Pereira, L.S.; Raes, D.; Smith, M. *Crop Evapotranspiration—Guidelines for Computing Crop Water Requirements—FAO Irrigation and Drainage Paper 56*, 9th ed.; Food and Agriculture Organization of the United Nations: Rome, Italy, 1998; ISBN 92-5-104219-5.
17. Li, X.; Kang, S.; Zhang, X.; Li, F.; Lu, H. Deficit irrigation provokes more pronounced responses of maize photosynthesis and water productivity to elevated CO₂. *Agric. Water Manag.* **2018**, *195*, 71–83. [CrossRef]
18. Grosso, C.; Manoli, G.; Martello, M.; Chemin, Y.H.; Pons, D.H.; Teatini, P.; Piccoli, I.; Morari, F. Mapping maize evapotranspiration at field scale using SEBAL: A comparison with the FAO method and soil-plant model simulations. *Remote Sens.* **2018**, *10*, 1452. [CrossRef]
19. Bastiaanssen, W.G.M.; Ali, S. A new crop yield forecasting model based on satellite measurements applied across the Indus Basin, Pakistan. *Agric. Ecosyst. Environ.* **2003**, *94*, 321–340. [CrossRef]
20. Liu, J.; Pattey, E.; Miller, J.R.; McNairn, H.; Smith, A.; Hu, B. Estimating crop stresses, aboveground dry biomass and yield of corn using multi-temporal optical data combined with a radiation use efficiency model. *Remote Sens. Environ.* **2010**, *114*, 1167–1177. [CrossRef]
21. Zwart, S.J.; Bastiaanssen, W.G.M. SEBAL for detecting spatial variation of water productivity and scope for improvement in eight irrigated wheat systems. *Agric. Water Manag.* **2007**, *89*, 287–296. [CrossRef]
22. Wagle, P.; Bhattarai, N.; Gowda, P.H.; Kakani, V.G. Performance of five surface energy balance models for estimating daily evapotranspiration in high biomass sorghum. *ISPRS J. Photogramm. Remote Sens.* **2017**, *128*, 192–203. [CrossRef]
23. Alvares, C.A.; Stape, J.L.; Sentelhas, P.C.; De Moraes Gonçalves, J.L.; Sparovek, G. Köppen’s climate classification map for Brazil. *Meteorol. Z.* **2013**, *22*, 711–728. [CrossRef]
24. INMET. Normais Climatológicas (1961–2018). 2019. Available online: <http://www.inmet.gov.br/portal/index.php?r=clima/normaisClimatologicas> (accessed on 5 March 2020).
25. Santos, H.; Jacomine, P.; Anjos, L.; Oliveira, V.; Lumberras, J.; Coelho, M.; Almeida, J.; Cunha, T.; Oliveira, J. *Embrapa: Sistema Brasileiro de Classificação de Solos*, 5th ed.; Embrapa, Ed.: Brasília-DF, Brasil, 2018; ISBN 9788570358004. Available online: <https://www.embrapa.br/solos/busca-de-publicacoes/-/publicacao/1094003/sistema-brasileiro-de-classificacao-de-solos> (accessed on 10 June 2019).
26. Yang, H.; Lee, Y.; Jeon, S.Y.; Lee, D. Multi-rotor drone tutorial: Systems, mechanics, control and state estimation. *Intell. Serv. Robot.* **2017**, *10*, 79–93. [CrossRef]

27. Mapir. Available online: <https://www.mapir.camera/products/survey3w-camera-red-green-nir-rgn-ndvi> (accessed on 16 January 2019).
28. Qgis; Version 2.18; Software For Geographic Information System; Open Source Geospatial Foundation: Chicago, IL, USA, 2016.
29. Rouse, R.W.H.; Haas, J.A.W.; Deering, D.W. Monitoring vegetation systems in the great plains with ERTS. *Third Earth Resour. Technol. Satell. Symp. Tech. Present. Nasa Sp-351* **1974**, *1*, 309–317.
30. Huete, A. A soil-adjusted vegetation index (SAVI). *Remote Sens. Environ.* **1988**, *25*, 295–309. [[CrossRef](#)]
31. García, P.; Pérez, E. Mapping of soil sealing by vegetation indexes and built-up index: A case study in Madrid (In Spain). *Geoderma* **2016**, *268*, 100–107. [[CrossRef](#)]
32. Gilabert, M.A.; González-Piqueras, J.; García-Haro, F.J.; Meliá, J. A generalized soil-adjusted vegetation index. *Remote Sens. Environ.* **2002**, *82*, 303–310. [[CrossRef](#)]
33. Zhang, L.; Niu, Y.; Zhang, H.; Han, W.; Li, G.; Tang, J.; Peng, X. Maize canopy temperature extracted from UAV thermal and RGB imagery and its application in water stress monitoring. *Front. Plant Sci.* **2019**, *10*, 1–18. [[CrossRef](#)]
34. Taiz, L.; Zeiger, E.; max Moller, I.; Murphy, A. *Plant Physiology & Development*; Sinauer Associates Inc.: Sunderland, MA, USA, 2015; ISBN 9781605352558.
35. Choudhury, B.J.; Ahmed, N.U.; Idso, S.B.; Reginato, R.J.; Daughtry, C.S.T. Relations between evaporation coefficients and vegetation indices studied by model simulations. *Remote Sens. Environ.* **1994**, *50*, 1–17. [[CrossRef](#)]
36. Monteith, J.L. Solar radiation and productivity in tropical ecosystems. *J. Appl. Ecol.* **1972**, *9*, 747. [[CrossRef](#)]
37. Coaguila, D.N.; Hernandez, F.B.T.; de Teixeira, A.H.C.; Franco, R.A.M.; Leivas, J.F. Water productivity using SAFER—Simple algorithm for evapotranspiration retrieving in watershed. *Rev. Bras. Eng. Agricol. E Ambient.* **2017**, *21*, 524–529. [[CrossRef](#)]
38. Teixeira, A.D.; de Miranda, F.R.; Leivas, J.F.; Pacheco, E.P.; Garçon, E.A.M. Water productivity assessments for dwarf coconut by using Landsat 8 images and agrometeorological data. *ISPRS J. Photogramm. Remote Sens.* **2019**, *155*, 150–158. [[CrossRef](#)]
39. Hatfield, J.L.; Asrar, G.; Kanemasu, E.T. Intercepted photosynthetically active radiation estimated by spectral reflectance. *Remote Sens. Environ.* **1984**, *14*, 65–75. [[CrossRef](#)]
40. Asrar, G.; Myneni, R.B.; Choudhury, B.J. Spatial heterogeneity in vegetation canopies and remote sensing of absorbed photosynthetically active radiation: A modeling study. *Remote Sens. Environ.* **1992**, *41*, 85–103. [[CrossRef](#)]
41. Moran, M.S.; Maas, S.J.; Pinter, P.J. Combining remote sensing and modeling for estimating surface evaporation and biomass production. *Remote Sens. Rev.* **1995**, *12*, 335–353. [[CrossRef](#)]
42. Toureiro, C.; Serralheiro, R.; Shahidian, S.; Sousa, A. Irrigation management with remote sensing: Evaluating irrigation requirement for maize under Mediterranean climate condition. *Agric. Water Manag.* **2017**, *184*, 211–220. [[CrossRef](#)]
43. Taghvaeian, S.; Chávez, J.L.; Hansen, N.C. Infrared thermometry to estimate crop water stress index and water use of irrigated maize in northeastern Colorado. *Remote. Sens.* **2012**, *4*, 3619–3637. [[CrossRef](#)]
44. Duchemin, B.; Hadria, R.; Erraki, S.; Boulet, G.; Maisongrande, P.; Chehbouni, A.; Escadafal, R.; Ezzahar, J.; Hoedjes, J.C.B.; Kharrou, M.H.; et al. Monitoring wheat phenology and irrigation in Central Morocco: On the use of relationships between evapotranspiration, crops coefficients, leaf area index and remotely-sensed vegetation indices. *Agric. Water Manag.* **2006**, *79*, 1–27. [[CrossRef](#)]
45. Rosa, R.D.; Ramos, T.B.; Pereira, L.S. The dual Kc approach to assess maize and sweet sorghum transpiration and soil evaporation under saline conditions: Application of the SIMDualKc model. *Agric. Water Manag.* **2016**, *177*, 77–94. [[CrossRef](#)]
46. Nascentes, R.F.; Carbonari, C.A.; Simões, P.S.; Brunelli, M.C.; Velini, D.; Duke, S.O. Low doses of glyphosate enhance growth, CO₂ assimilation, stomatal conductance and transpiration in sugarcane and eucalyptus. *Pest Manag. Sci.* **2017**, *74*, 1197–1205. [[CrossRef](#)]
47. Kim, T.-H.; Böhmer, M.; Hu, H.; Nishimura, N.; Schroeder, J.I. Guard cell signal transduction network: Advances in understanding abscisic Acid, CO₂, and Ca²⁺ Signaling. *Annu. Rev. Plant Biol.* **2010**, *61*, 561–591. [[CrossRef](#)]
48. Kang, S.; Zhang, F.; Hu, X.; Zhang, J. Benefits of CO₂ enrichment on crop plants are modified by soil water status. *Plant Soil* **2002**, *238*, 69–77. [[CrossRef](#)]

49. Driscoll, S.P.; Prins, A.; Olmos, E.; Kunert, K.J.; Foyer, C.H. Specification of adaxial and abaxial stomata, epidermal structure and photosynthesis to CO² enrichment in maize leaves. *J. Exp. Bot.* **2006**, *57*, 381–390. [[CrossRef](#)] [[PubMed](#)]
50. Campos, I.; González-Gómez, L.; Villodre, J.; González-Piqueras, J.; Suyker, A.E.; Calera, A. Remote sensing-based crop biomass with water or light-driven crop growth models in wheat commercial fields. *Field Crop. Res.* **2018**, *216*, 175–188. [[CrossRef](#)]
51. Twohey, R.J.; Roberts, L.M.; Studer, A.J. Leaf stable carbon isotope composition reflects transpiration efficiency in *Zea mays*. *Plant J.* **2019**, *97*, 475–484. [[CrossRef](#)] [[PubMed](#)]
52. Fandiño, M.; Cancela, J.J.; Rey, B.J.; Martínez, E.M.; Rosa, R.G.; Pereira, L.S. Using the dual-K c approach to model evapotranspiration of *Albariño* vineyards (*Vitis vinifera* L. cv. Albariño) with consideration of active ground cover. *Agric. Water Manag.* **2012**, *112*, 75–87. [[CrossRef](#)]
53. Yang, Y.; Xu, W.; Hou, P.; Liu, G.; Liu, W.; Wang, Y.; Zhao, R.; Ming, B.; Xie, R.; Wang, K.; et al. Improving maize grain yield by matching maize growth and solar radiation. *Sci. Rep.* **2019**, *9*, 1–11.
54. Killi, D.; Bussotti, F.; Raschi, A.; Haworth, M. Adaptation to high temperature mitigates the impact of water deficit during combined heat and drought stress in C3 sunflower and C4 maize varieties with contrasting drought tolerance. *Physiol. Plant* **2017**, *159*, 130–147. [[CrossRef](#)]
55. Trout, T.J.; Dejonge, K.C. Water productivity of maize in the US high plains. *Irrig. Sci.* **2017**, *35*, 251–266. [[CrossRef](#)]
56. Wang, Y.; Janz, B.; Engedal, T.; De Neergaard, A. Effect of irrigation regimes and nitrogen rates on water use efficiency and nitrogen uptake in maize. *Agric. Water Manag.* **2017**, *179*, 271–276. [[CrossRef](#)]
57. Liao, C.; Wang, J.; Dong, T.; Shang, J.; Liu, J.; Song, Y. Using spatio-temporal fusion of Landsat-8 and MODIS data to derive phenology, biomass and yield estimates for corn and soybean. *Sci. Total Environ.* **2019**, *650*, 1707–1721. [[CrossRef](#)]



© 2020 by the authors. Licensee MDPI, Basel, Switzerland. This article is an open access article distributed under the terms and conditions of the Creative Commons Attribution (CC BY) license (<http://creativecommons.org/licenses/by/4.0/>).